

# International Conference on Space Optics—ICSO 2018

Chania, Greece

9–12 October 2018

*Edited by Zoran Sodnik, Nikos Karafolas, and Bruno Cugny*



## ***Fire detection from LEO: trade-offs for selection of spectral bands and a wide-swath optical design using MWIR and visible bands***

*Dan Lobb*

*Rachel Bird*

*Martin Wooster*

*Amanda Regan*



icso proceedings



# Fire detection from LEO: trade-offs for selection of spectral bands and a wide-swath optical design using MWIR and visible bands

Dan Lobb<sup>a</sup>, Rachel Bird<sup>b</sup>, Martin Wooster<sup>c</sup>, Amanda Regan<sup>d</sup>

<sup>a</sup>DLOptics Ltd, 25 Marlings Park Avenue, Chislehurst, UK, BR76QN; <sup>b</sup>Surrey Satellite Technology Ltd, Tycho House, 20 Stephenson Road, Guildford, UK, GU2 7YE; <sup>c</sup>King's College London, Strand, London, UK, WC2R 2LS; <sup>d</sup>ESA-ESRIN, Largo Galileo Galilei, 1, 00044 Frascati RM, Italy

## ABSTRACT

The paper relates to design of a sensor, operating on a platform Low-Earth Orbit, that will detect and measure actively burning fires on Earth surface. Trade-offs for selection of spectral bands are covered, concentrating on options using cooled detectors. A system using only two mid-wave infrared (MWIR) bands is shown to be viable; it will have significant cost advantages compared with a system that also uses long-wave infrared (LWIR), since it requires smaller optics for spatial resolution at the diffraction limit, and less-extreme detector cooling. Imaging in at least one visible band will allow identification of false detections due to sun glint, so that small fires can be positively identified in sunlight.

A proposed sensor will operate in pushbroom mode. The design uses a single area-array MWIR detector with a 1280 x 1024 element format. A swath approaching 10,000 pixels wide is provided by sub-dividing the swath between 8 telescopes that image onto separate sets of strip filters and detector rows. This allows a total swath width approaching 1000km wide to be scanned at 100m ground sample distance (GSD). The relatively small GSD, and use of multiple detector rows for each swath-section and band, will provide a capability for detection of small fires, with radiant powers in the range 0.5 to 1.0 MW. Wide swath will maximize statistical data collected by the sensor, and will also be of potential interest for development of constellation providing global fire monitoring.

**Keywords:** Earth observation, fire detection, fire radiant power, mid-wave infrared

## 1. INTRODUCTION

This paper reports the main results of a study performed by Surrey Satellite Technology Ltd and University College London for the European Space Agency, completed in December 2015. The study was focused on design of a sensor, flown on a platform in low-Earth, that will gather data on actively burning fires. Data on fires is important for analyses of land-cover changes, including forest clearance, biogeochemical cycling, and for research on generation of greenhouse gasses, reactive gasses and aerosols. Volcanoes, gas flares and other high temperature events would also be targeted by a fire measurement system. The baseline mission concept included operation in convoy with the ESA Sentinel satellites<sup>1</sup>, for example complementing data provided by the SLSTR instrument on Sentinel 3, which also has fire-detection capabilities<sup>2</sup>. The sensor concept, as developed in the study, provides fire measurement over a wide swath. This optimizes the statistical data volumes that the sensor can provide, but would also limit the numbers of satellites required in a constellation aiming at global fire monitoring.

Section 2 below discusses selection of spectral bands for the fire-measurement sensor, and the associated selection of detector types. There is a preference for use of two MWIR bands, centered at 3.5 $\mu$ m and 4.65 $\mu$ m, which together will provide measurement of fire radiant powers and temperatures. An MWIR-only system will have significant cost advantages compared with a system that also uses LWIR. It requires smaller optics for spatial resolution at the diffraction limit, and less-extreme detector cooling. A visible band is added to allow identification of false detections due to sun glint, so that small fires can be positively identified in sunlight. Visible imaging will also provide context for fires.

Section 3 below describes the proposed sensor optical system. The sensor operates in pushbroom mode from a nominal LEO altitude of 814km. Aims for optical design include minimizing GSD, which determines the minimum fire sizes that can be detected and measured. Wide swath is desirable for maximizing statistical data collected by a single sensor and is potentially valuable for global fire detection and monitoring from a satellite constellation. The design uses a single area-array MWIR detector with a 1280 x 1024 element format. A swath approaching 10,000 pixels wide, at 100m GSD is provided by sub-dividing the swath between 8 telescopes that image onto separate sets of detector rows. Strip filters located in an intermediate image plane isolate the two required MWIR bands for each field section. Multiple detector rows are available for each field segment and spectral band, providing useful spatial oversampling. Very wide dynamic range is required to cover both detection of small fires and measurement of large fires. The design provides multiple (ghost) images separated along-track at progressively lower transmission so that large fire radiant powers can be measured within detector saturation.

Section 4. below summarizes system design, physical parameters and performance. The minimum detectable fire radiant power will be in the range 0.5 to 1.0 MW.

## 2. DETECTORS AND SPECTRAL BAND SELECTION

Fire detection from space is generally based on measurement of scene radiances in selected thermal infrared spectral bands in the MWIR and LWIR atmosphere windows <sup>2</sup> (roughly 3 $\mu$ m to 5 $\mu$ m and 8 $\mu$ m to 12 $\mu$ m). Thermal radiances of fires, at typical temperatures ranging from 600K to 1300K <sup>3</sup>, are much higher than radiances of typical background scenes, so that detection of large fires does not present serious problems. However, the aim is also generally to detect fires subtending a small fraction of the detector pixel. Pixel signals are commonly characterized by “brightness temperature (BT)”: this is the uniform temperature of a pixel, treated as a black body, that would give the same signal in the specified spectral band.

Current fire detection systems measure and compare signals in a MWIR band and a LWIR band. The key detection metric used in active fire detection algorithms is the MWIR-LWIR brightness temperature difference, which is elevated at pixels containing sub-pixel actively burning fires <sup>4</sup>. Since this difference is also non-zero at non-fire "background" pixels, because for example of atmospheric and surface emissivity effects, the MWIR-LWIR brightness temperature difference of the pixel being tested is usually compared to that present at the surrounding ambient background pixels. If a large enough difference exists between these two values – i.e. if the metric  $(BT_{MWIRfire} - BT_{LWIRfire} - (BT_{MWIRback} - BT_{LWIRback}))$  is sufficiently high – then the pixel can be considered likely to contain an active fire <sup>4</sup>. The most sensitive active fire detection algorithms can perhaps detect cases where a 5 or 6 K difference is seen in this metric, though 10 K is more commonly used: this equates to a fire pixel proportion of roughly  $10^{-3}$  to  $10^{-4}$ , depending upon the fire temperature. (Hotter fires can be detected covering a smaller pixel proportion than cooler fires.)

### 2.1 Detection capabilities using only MWIR bands compared with MWIR and LWIR bands

A main interest in the study performed for ESA has been the potential for replacement of the LWIR band with a second MWIR band. The initial reasons for this interest are related partly to detector options. Microbolometer arrays were initially considered, since they have the advantage that they do not require cooling – this option has been discarded mainly because of low sensitivity: very large optics are required to feed the detectors at short f-numbers. The likely cooled photo-detectors are mercury cadmium telluride (MCT) arrays. The advantages of MWIR over LWIR MCT arrays are:

- (a) larger detector formats are generally available, leading to the possibility of wider swath widths for the sensor and/or smaller GSDs leading to detection of smaller fires,
- (b) less extreme cooling is required: typically around 150K for MWIR compared with <100K for LWIR and
- (c) smaller optical apertures are required (roughly by a factor 2.5) for a given diffraction limited GSD: this has a significant impact on mass and envelope of sensor optics.

To assess the viability of a system based on two MWIR bands the brightness-difference detection metric for a MWIR/LWIR sensor:  $BT_{MWIRfire} - BT_{LWIRfire} - (BT_{MWIRback} - BT_{LWIRback})$ , has been compared with an equivalent metric for two MWIR bands, MWIR1 and MWIR2:  $BT_{MWIR1fire} - BT_{MWIR2fire} - (BT_{MWIR1back} - BT_{MWIR2back})$ . Results for the comparison are shown in Figure 1. Figure 1(a) shows the comparison with two MWIR bands that are relatively closely spaced in wavelength (3.5 and 3.9  $\mu$ m). The curve lies mainly below the 1:1 line, indicating that detection capability

using these two MWIR bands is worse than for the LWIR-MWIR combination. Figure 1(b) shows the comparison with two MWIR bands that are spaced further apart: 3.5 and 4.65  $\mu\text{m}$ . In this case the brightness temperature difference (x-axis for the MWIR-LWIR baseline) lies above the 1:1 line for all fire temperatures, up to a BT differences over 20 K. This indicates that the detection ability for the same fire temperature and sub-pixel size using these two MWIR bands can be as good, or better, than if a MWIR and LWIR band were used conventionally. Above a MWIR-LWIR BT difference of 25 K the curves fall below the 1:1 line, but this is already a region where fire detection is becoming much more unambiguous, with strong MWIR signals above the background.

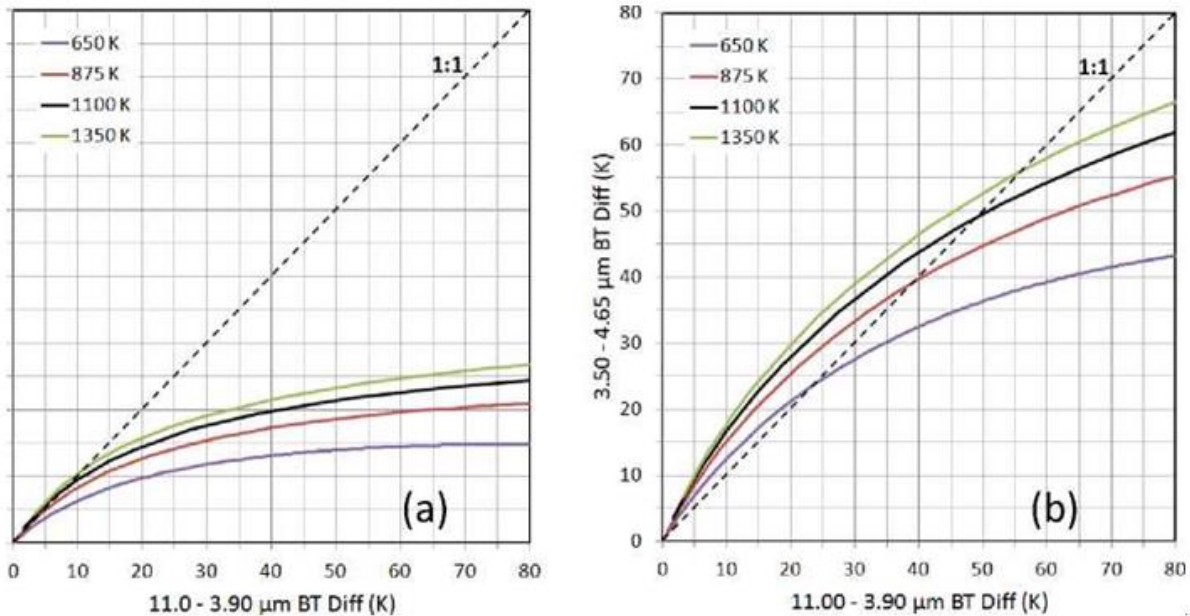


Figure 1: Simulations of top-of-atmosphere pixel integrated brightness temperature differences ( $B_{\text{BAND1fire}} - B_{\text{BAND2fire}} - (B_{\text{BAND1back}} - B_{\text{BAND2back}})$ ) compared between MWIR and LWIR bands (horizontal axis) and two MWIR band (vertical axis). Simulated for sub-pixel fires covering a range of pixel proportions and with different active fire temperatures (650 - 1350 K). A 300 K background temperature and a 1976 US Standard Atmosphere is assumed, with simulations conducted using MODTRAN 5. (a) 3.50 - 3.90  $\mu\text{m}$  BT difference vs. 11.0 - 3.9  $\mu\text{m}$  BT difference, (b) 3.50 - 4.65  $\mu\text{m}$  BT difference vs. 10.0 - 3.9  $\mu\text{m}$  BT difference.

## 2.2 Measurement of fire radiant power and temperature

Fire radiant power (FRP) is typically measured using the MWIR band of a system with MWIR and LWIR bands, since radiance at around 3.9  $\mu\text{m}$  varies almost linearly with FRP over typical fire temperature ranges. This is shown in Wooster et al (2005)<sup>4</sup> where the 3.9  $\mu\text{m}$  spectral radiance from fires of varying pixel proportion and varying temperature (650 - 1350 K) are simulated on a 300 K background and the FRP calculated from these radiances (no atmospheric effects are included). To check that MWIR bands at 3.5  $\mu\text{m}$  and/or 4.65  $\mu\text{m}$  can also be used to estimate FRP, the same computation has been performed with the waveband shifted to 3.5  $\mu\text{m}$  and 4.65  $\mu\text{m}$ . Figure 2 shows the strong linear relationship between the FRP's derived from the two new MWIR wavelength measurements, and the measurement at 3.9  $\mu\text{m}$ . The high coefficient of variation ( $r^2$ ) between both the 3.5  $\mu\text{m}$ - and 4.65  $\mu\text{m}$ -derived FRP values, and the 3.9  $\mu\text{m}$ -derived FRP, indicates that either of these two alternative wavebands could likely be used to derive FRP estimates, after the observed radiances have been atmospherically corrected. It may be preferable to use the 4.65  $\mu\text{m}$  measurement due to the significantly lower solar reflected radiation component within this waveband compared to the 3.5  $\mu\text{m}$  waveband.

## 2.3 Discrimination against sun glints using two thermal IR bands

As outlined in 2.1 above, fire detection using BTDs is expected to work with two MWIR bands at least as well as with one MWIR band and one LWIR band. However, this analysis so far ignores effects of solar reflections. The main issue for the MWIR bands is expected to be sun glints: specular surface reflections from water surfaces, and occasionally from glass and metal surfaces of man-made structures and vehicles. (Diffuse bulk reflections can be strong in the visible range, but high diffuse emissivities and low diffuse reflectances are generally expected in thermal IR bands for both fires

and background.<sup>5,6)</sup> The MWIR intensities of sun glints can be significant compared with small fires, particularly at the shorter MWIR wavelengths. For example a crude calculation at 3510nm indicates that a sun glint giving a pixel-averaged reflection equivalent to 10% diffuse reflectance (Lambertian polar distribution) would raise BT in this band by 24K at 300K. The same glint would raise the BT in the 4653nm band by only 2.5K at 300K.

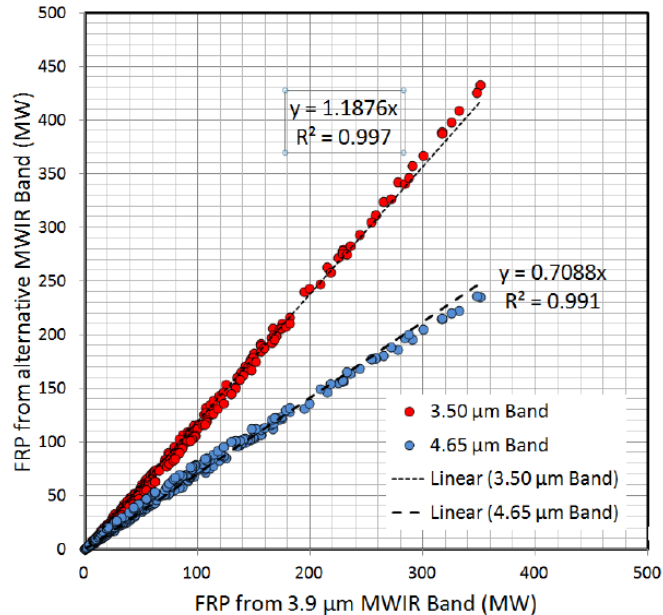


Figure 2 Simulations of FRP retrieved from spectral radiances simulated in two MWIR bands

Glints from water produce a very wide range of radiances depending on the roughness of the water and the angle of view with respect to sun-specular. Very flat water produces a diffuse-equivalent reflectance of about 100,000% over a half-degree spread. A reflection from flat glass would produce a radiance equivalent to diffuse reflectance of about 400,000%. Effective reflectances are of course reduced for sub-pixel areas, so that a 1m square of flat glass in a 100m square pixel will produce diffuse equivalent reflectance of 40% in the sun glint direction.

Operation only on the dark side of the orbit would of course eliminate solar reflectance effects, but this would be considered a serious limitation on mission value. Using only the BT difference metric with any two thermal bands, typical sun-glint signals in the shorter waveband will often be interpreted as small fires. An additional approach will be required to allow reliable detection of small fires in daylight. Figure 3 illustrates a possible approach and the likely problems for a system limited to two MWIR bands. Here we address a pixel with a brightness temperature of 315K at 4653nm (band 2), in a scene at an average temperature 300K. We calculate the black-body signal anomaly in band 2 implied by the 15K difference in BT, and calculate the signal that we would expect in band 1 (at 3510nm) on different assumptions about the temperature of the anomaly in the pixel: fires at 650K or 1350K, or a sun glint at 6000K. The simplifying assumptions include: (a) glint reflectance and background emissivity are equal in the two MWIR bands and (b) the atmosphere has effectively 100% transmission in both bands. The calculated signals in band 1 are plotted relative to the 300K background signal. However the plots are extended to show the results on a range of assumptions for the true background temperature in the pixel: between -5K and +5K with respect to the assumed 300K scene average.

As indicated in Figure 3, the increased signal in band 1 due to sun glint is typically 60% above the increase that would be expected from the hottest fires, allowing sun-glint to be suspected. However, the plots show that sun-glint cannot be identified reliably in the presence of significant uncertainty in the true background temperature of the target pixel. In the example shown, the predicted signal in band 1 is the same for sun-glint with a +5K background delta as for a hot fire with a -5K background delta. The same uncertainty range (at 15K delta BT in band 2) also produces a full-range uncertainty in prediction of fire temperatures. It should also be noted (a) that significant errors in relative signal levels

will be introduced by mis-registration between sensor images in the two bands (including temporal mis-registration since sun glint can be transient) and (b) errors will be introduced by differences in emissivities glint-reflectances and atmosphere transmission between the two MWIR bands.

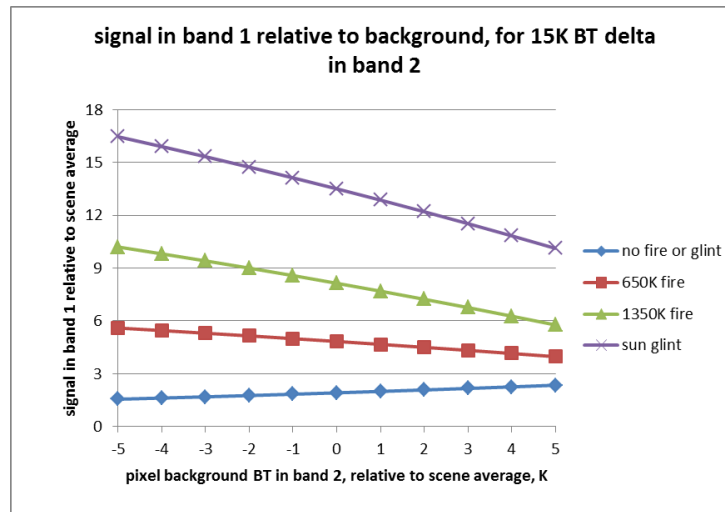


Figure 3: Signal expected from the target pixel in band 1 (3510nm) if the scene average temperature is 300K and there is a measured BT of 315K in the target pixel in band 2 (4653nm). Target-pixel signal in band 1 is plotted relative to the 300K scene-average in band 1. The signal in band 1 is calculated on the assumptions that the raised BT in band 2 is produced (a) by a fire at 650K, (b) by a fire at 1350K, (c) by a sun glint. The relative signals are plotted against deltas in the true background temperature of the target pixel with respect to the scene average (i.e at true target-pixel background temperatures from 295K to 305K). Also shown is the relative signal in band 1 with a 15K mean anomaly, plus the same deltas.

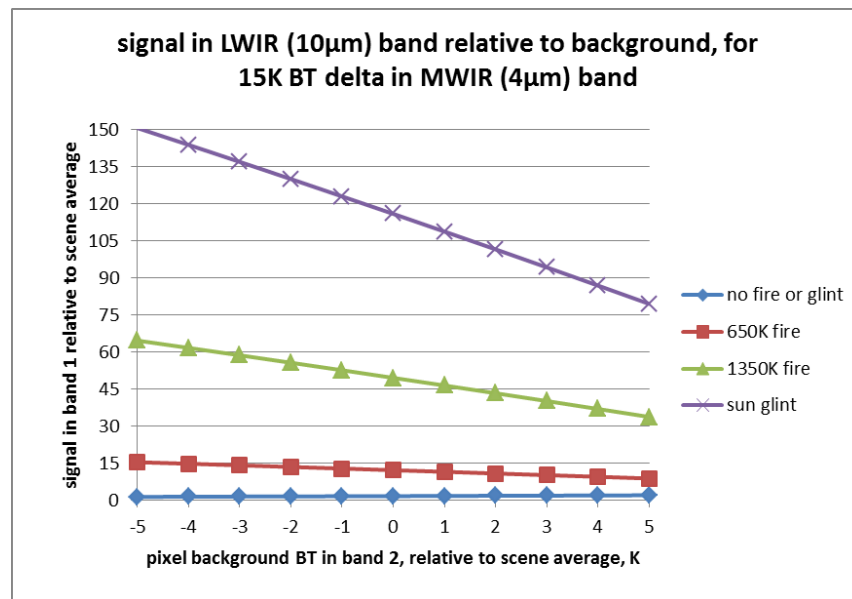


Figure 4: As Figure 3, but with band 1 at 4000nm and band 2 at 10,000nm

Use only of two MWIR bands has therefore been provisionally rejected. A similar approach (comparing excess BT levels in the shorter wave band for a given BT excess in the longer waveband, for fires and sun-glint) has also been applied to a system with a single MWIR band and a LWIR band: results are show in Figure 4. As expected, use of longer wavelengths will provide better immunity to effects of sun glint. However, uncertainties much over  $\pm 5K$  in the true background temperature of target pixels will again affect discrimination between sun glint and the hottest fires. If a LWIR band were an easy addition, it would probably be included. However, to work effectively, it would need similar

GSD to the MWIR band(s). This would require a much larger aperture than a MWIR-only system (typically by a linear factor 2.5 due to the diffraction limit, as noted above). The practical impact is probably that GSDs would be increased in size to limit the sensor size, with impacts on minimum detectable fire radiative power (FRP). The analysis does not make a strong case for inclusion of a LWIR band.

#### 2.4 Use of a visible channel to identify sun glint: minimum detectable radiant power

In the preferred sensor design, a visible channel is likely to be included for several possible functions in addition to discrimination against sun glint, including cloud masking and providing images of areas with fires in progress. Spatial and temporal registration of visible and thermal channels may be considered essential for sun glint rejection, since highly directional glint from small flat areas (typically glass and smooth water) will be seen as rapidly-changing from the satellite (potentially at vignetted intensity or complete missed by the visible channel). However, the minimum angular spread of glint will equal the angular subtense of the sun, so that it will be reasonable to allow an along-track mis-registration up to  $0.25^\circ$  (half sun subtense) between instrument MWIR and visible fields – corresponding to 3.5km on ground or about 0.5s temporal registration error.

Simplistically, the visible channel may be used to discard all pixels that indicate visible diffuse-equivalent (Lambertian) reflection above an absolute level about 120%, that would be produced only or partly by sun glint. A glint at a diffuse-equivalent level of 120% corresponds to a delta brightness temperature of 22K at 300K in a MWIR band at 4653nm. I.e. all sun-glint affected pixels are in theory discarded, from a scene at a uniform 300K temperature, if we also exclude those showing a BT below 322K in the longer MWIR band. (Use of the shorter MWIR band would be less effective.) With margins for background non-uniformity, this probably means that we ignore pixels at BT levels less than about 25K above the average background at 4653nm. This would correspond to a fractional fire area of 0.0046 for a fire at 650K, or 0.00036 for a fire at 1350K. For pixels 100m square, these fractional fire areas would be 45m<sup>2</sup> at 650K or 3.5m<sup>2</sup> at 1350K. The equivalent FRPs are 0.45MW at 650K and 0.65MW at 650K.

#### 2.5 Other possible strategies against sun glint

An approach closer to classical methods might use a brightness temperature different (BTD) between two thermal IR bands (together with a visible channel threshold) rather than a simple threshold based on difference-from-background in any single thermal band. This would in principle remove or reduce the effects of background temperature uncertainty (if uncertainties in ground emissivity and atmosphere transmission are ignored). However, if the visible channel fails to discriminate against relatively high levels of glint – for example 120% diffuse equivalent – potential glint errors in the MWIR bands will dominate the uncertainties due to background non-uniformity. It therefore does not seem clear that thresholding against sun glint, based on visible signal plus a BTD between two MWIR bands, would be useful.

Other possible methods to reduce false fire-detections due to sun glint might include (a) pitching the platform to avoid peak sun-glint from water, or ignoring scene areas within a TBD angle of peak sun-glint, (b) detecting rapid changes in signals over an along-track field: this will indicate highly-directional glint, (c) discarding data from areas in which false fire detections have been recorded on previous orbits.

### 3. SENSOR DESIGN DEVELOPMENT

Preliminary requirements and design-assumptions for a fire detection and measurement sensor operating in two MWIR bands are:

- The sensor shall image Earth from a satellite in LEO at a nominal altitude of 814km (potentially operating in convoy with Sentinel 3).
- The sensor shall measure Earth radiance in MWIR bands centered at 3.5 $\mu$ m and 4.65 $\mu$ m providing detection of fires, measurements of fire radiant powers and estimates of fire temperatures.
- The sensor shall include a visible channel registered with a MWIR channel for detection of sun glint, and also to provide pictures of fire areas and support cloud-cover mapping.
- The sensor shall operate during day and night parts of the orbit, taking account of effects of sun glint and other reflected sunlight during day.
- The sensor shall image land areas continuously: the swath center is assumed to be at nadir.

- Sensor noise-equivalent delta-temperatures in the two spectral bands shall be <1K at 300K background (black-body) temperature.
- Sensor ground sample distance shall be minimized, with a target of 100m.
- Sensor swath width shall be maximized. A 1000km swath will provide an average re-visit time of 1.5 days (constellation of ~20 satellites to detect fires within 2 hours ignoring cloud cover).
- The mission lifetime shall be >7.25 years (c.f. Sentinel 3).

### 3.1 MWIR detector selection and method of use

Optical design concepts for thermal detection and assessment of fires are driven largely by detector capabilities as noted in 2.1 above. The baseline concept works only in MWIR bands (plus visible for sun-glint identification) partly because available LWIR detectors have fewer array elements. Linear array detectors could be used effectively in a push-broom scanning system, but area arrays tend to be preferred partly because manufacturers have relatively little interest in development of linear arrays for thermal bands. In the baseline design, the MWIR detector is the Selex SuperHawk, which has 1280 columns that will be assigned to spatial resolution, and 1024 rows. The detector element size is 8 $\mu$ m square. The large number of rows will be used in several ways:

- (a) Strip filters will be used to define the required MWIR spectral bands: pushbroom operation will typically scan the scene sequentially in the two bands,
- (b) Several telescopes (baseline 8) will image the separate sections of the swath onto separate sets of detector rows (baseline 16 sections for two spectral bands in each of 8 swath sections). The telescopes will image swath sections spaced across-track, providing a total swath width approaching 8 x 1280 pixels wide,
- (c) Several detector rows will be read out for each waveband and swath section. This provides an opportunity to introduce spatial oversampling of the scene. Across-track oversampling will be introduced by rotating the detector so that columns do not align with the along-track movement of the scene image. Along-track oversampling will be introduced by non-synchronous read-out with respect to along-track image movement. This ensures that some of the samples record near-centered fire images at near-maximum levels: an important advantage for initial thresholding to identify likely fires.
- (d) Multiple reads will be processed to improve noise-equivalent temperature differences (NEDTs) for identified fires, improving FRP and temperature estimates.

### 3.2 Baseline MWIR optical design

A baseline optical design, using 8 telescopes with one detector, is shown in Figure 5. The beams collected by the 8 telescopes are shown in separate colours. The beam from each telescope is folded at two flat mirrors and one reflecting prism: the 8 beams form parallel strip images on a set of filters that define the required spectral bands. The combined image is then relayed onto the detector by a relay lens. The detector dewar and cooling engine are included at approximately correct scale. Most of the optics – including the fold mirrors and prisms, the relay lens and the detector – are in a common plane. However, the telescope lenses are out of the main optics plane, as shown in Figure 6. The first fold mirror on each telescope axis is angled to generate 8 different view-directions across-track. The 8 fields, each 8.8° degrees wide, nominally abut across-track, producing a 70° total field.

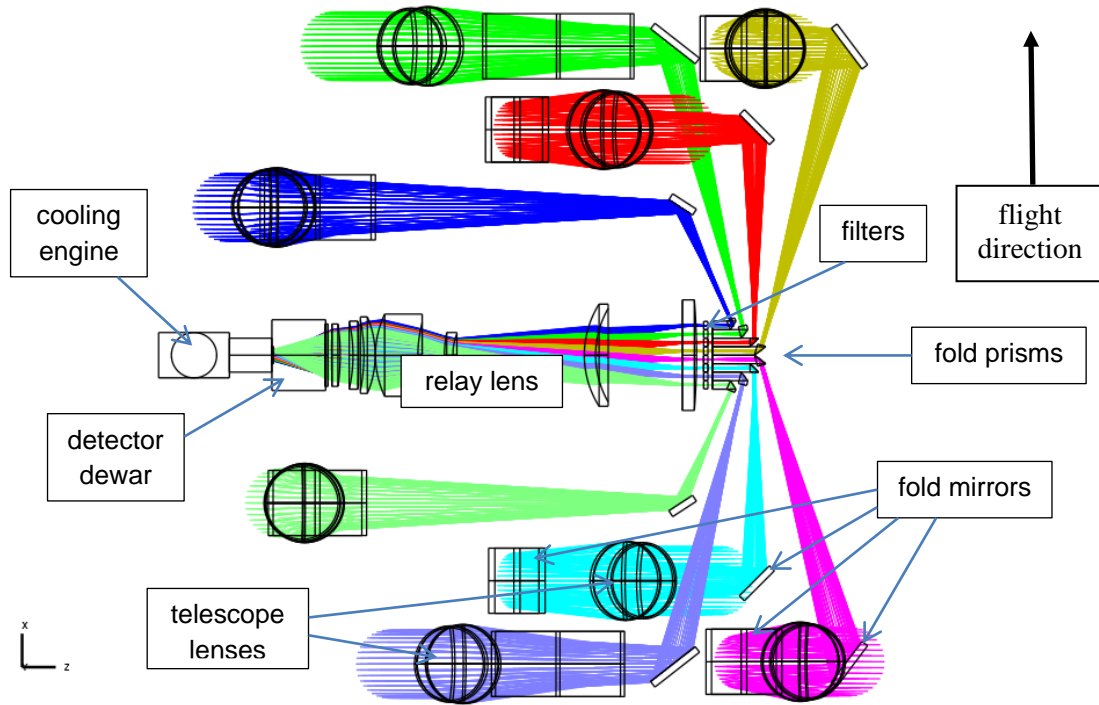


Figure 5: Fire monitoring optics – view on nadir axis. Optics dimensions excluding structure: 500mm along-track x 500mm across-track.

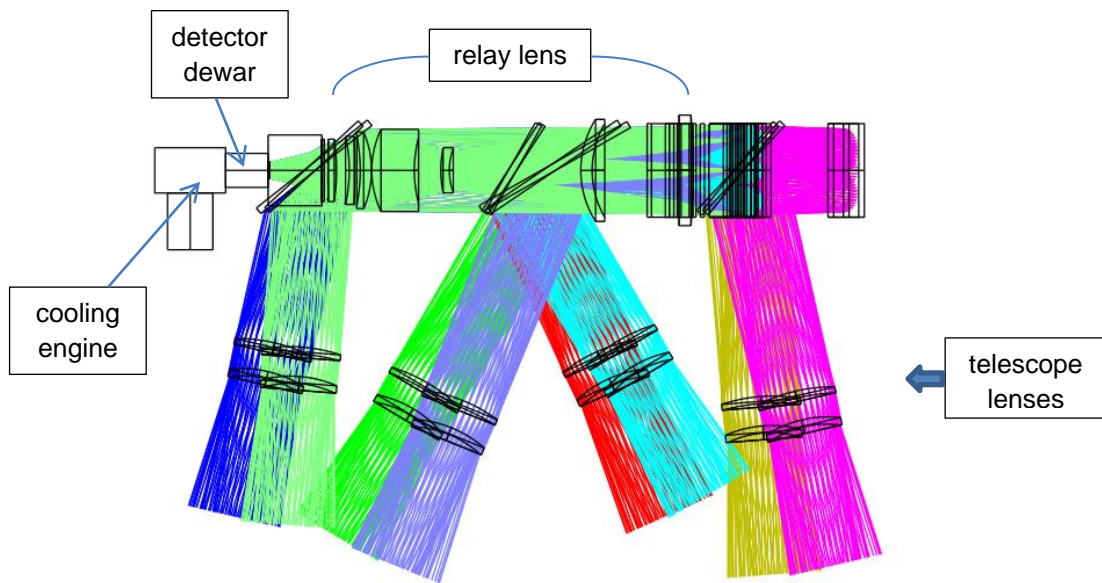


Figure 6: Fire monitoring optics – view along-track. Optics dimension on nadir axis, excluding structures: 240mm

Shaded models are shown in Figures 7 and 8. For clarity, a single telescope channel is shown in Figure 7 and the complete optical system in Figure 8.

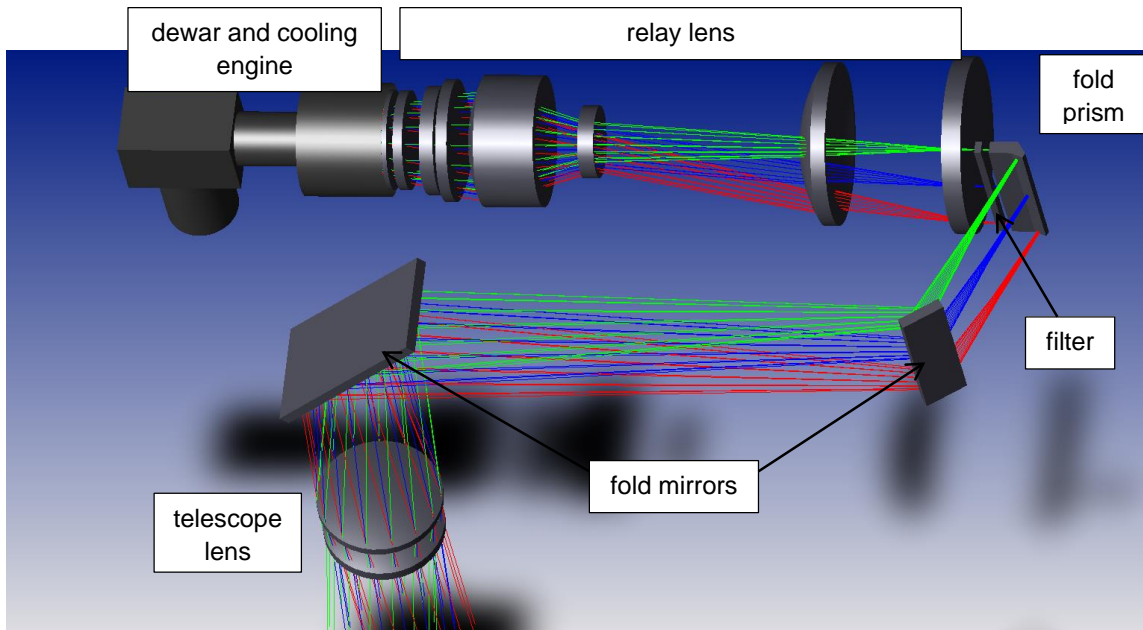


Figure 7: Fire monitoring optical systems – shaded view of a single telescope channel

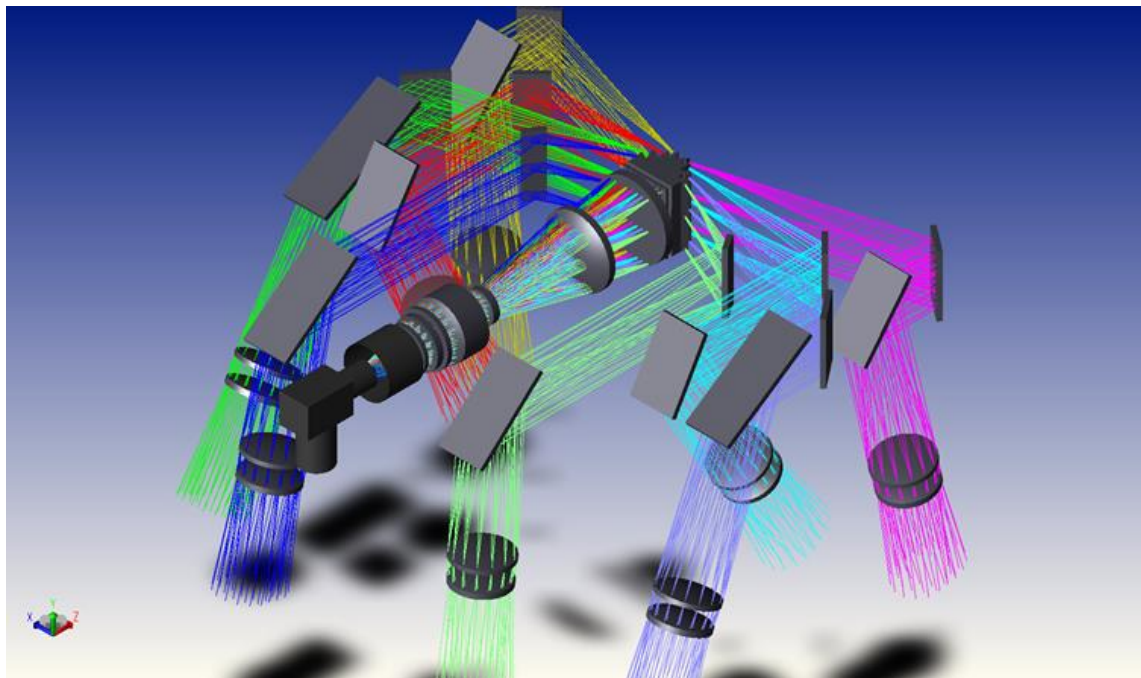


Figure 8: Fire monitoring optical systems – shaded view of all channels

### Telescopes

The telescope lenses have focal lengths of 391mm: each has an  $8.8^\circ$  sub-swath field, producing an image 60mm wide at the filters. The total image area at the filters is 60mm x 48mm. This image area is relayed onto the detector (8mm x 10mm active area) at x 1/6 magnification. The telescope apertures are 48mm diameter, so that the primary image on the filters is formed at f/8.15; the image on the detector is formed at f/1.36. The telescopes are two-element lenses with one surface aspherised – using silicon and germanium to provide chromatic correction. Resolution of the scene images formed on the filters is diffraction limited over the  $8.8^\circ$  fields and in each of the two spectral bands. The baseline design, as detailed at present, provides the same angular field and angular resolution for all 8 across-track sections of the

swath, since the 8 telescopes are identical. In a more-developed design, there will be an option to use a set of 4 focal lengths for the 8 telescopes, with increasing focal lengths for the extreme swath-sections: this will compensate for oblique viewing, providing a more-uniform GSD across the total swath width.

### Fold prisms and filters

Figure 9 shows a section through the fold prisms and filters. Silicon prisms are used, rather than simple mirrors, to reduce the convergence angle of beams in the fold paths: the high refractive index of the prisms reduces vignetting losses in the useful strip-image widths at the filters. Each of the 8 sub-swath image sections will be split between two strip filters, as shown in Figure 9. Each silicon filter is nominally 3mm wide along-track and 60+mm long across-track. The filters are provisionally 10mm thick, and cemented on 10mm x 60+mm faces to provide a robust assembly that can be mounted relatively easily. Band-pass filter coatings will be applied on the inside faces (detector sides) of the substrates, with anti-reflection coatings on outer faces.

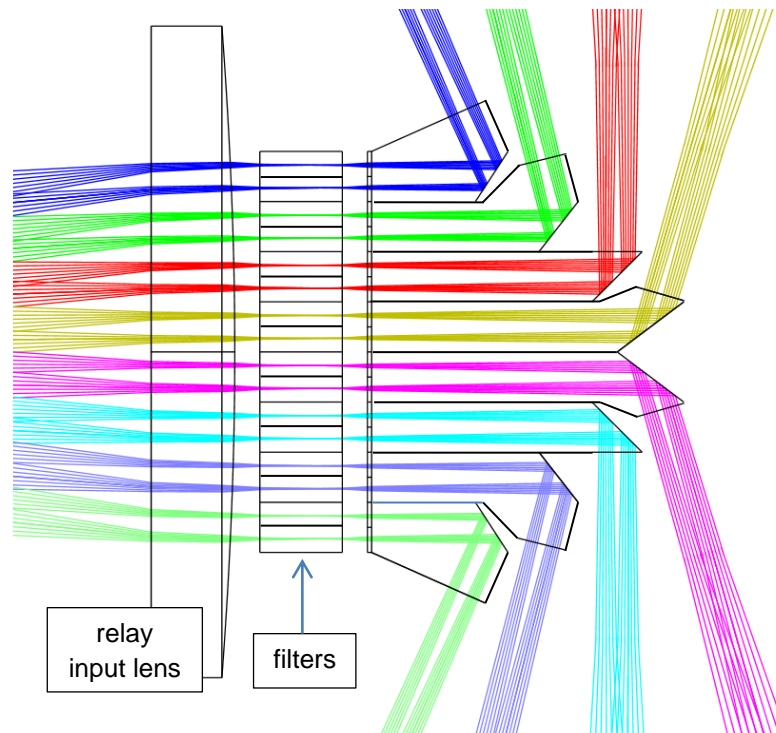


Figure 9: Fold prisms and filters

### Spatial oversampling using detector rotation and asynchronous read-out

The separations between the 8 fields at the filters are 6mm (so that 8 channels use the whole available detector area after x 1/6 magnification). 1.7mm of each 6mm strip is lost due to calculated vignetting; this will be increased to approximately 2mm with allowances for misalignments etc. Each swath-section and band can therefore be assigned up to 2mm image width at the primary image – this corresponds to 0.33mm at the detector, or 41 detector columns. In effect this allows the system to collect up to 41 samples from each ground point, in each of the two MWIR bands. All these samples can eventually be processed to improve signal to noise ratios. However, an initial thresholding algorithm is likely to be based on maximum signal received at any individual detector pixel. It will therefore be desirable to arrange that any potential fire image is close to the center of at least one pixel, in the available set of around 41 pixels. Provisionally this will be achieved by:

- Rotating the detector 1.6° degrees with respect to the direction of image movement across the detector (assuming yaw steering), so that successive detector rows see a fire at 1/36 pixel increments across-track,
- Reading out the detector 7 times in the period taken to scan 6 pixels.

This will be expected to ensure that one pixel is read out with any fire <1/12 pixels from center, both along-track and across-track.

### Relay lens and dewar

The current relay lens design has 5 silicon elements and two germanium elements; the first (field lens) element and one other element have an aspheric surface. The performance of the relay in combination with each telescope is diffraction limited in each of the two MWIR wavebands. (Little effort has been applied to relay optimization, so that the lens may be simplified with more work.) The effective aperture of the optical system, in all telescope fields, will be at the aperture of the dewar. In the current design, the aperture is 37.6mm from the detector plane, with a diameter of 27.7mm, defining the system f/number at 1.36. (The dewar cold shield will be modified to set the required aperture.)

### Ghost image generator – dealing with detector saturation

Detector saturation can present problems for measurements on relatively large fires <sup>7</sup>. A fire at 1350K filling the pixel would give calculated sample signals of 1100M electrons in the 3150nm band and 820M electrons in the 4653nm band. This compares with a nominal detector saturation level of 5M electrons for the selected detector. It will be desirable to increase the effective system dynamic range by at least 2 orders of magnitude. The preferred method involves placing a transmitting wedge immediately outside each of the 8 telescopes, as indicated in Figure 10. (This modification is not included in Figures 5 to 8.) Multiple reflections inside the wedge will produce ghost images of the scene superimposed on the main image. Using, for example, uncoated zinc selenide, the single surface reflection will be 14.8% and the relative intensities of ghosts produced by double and quadruple reflections will be 2.2% and 0.048%. If the wedge angle is set at  $0.1^\circ$  in the along-track direction, the system will see the main image at nadir, superimposed on images leading along-track at angles of  $0.45^\circ$ ,  $0.9^\circ$  etc. (separations on ground of 6.4km at 814km altitude). If the main image is recorded as saturating the detector, the following double-reflection or quadruple-reflection image will be recorded within saturation. The ghost images will not be expected to interfere significantly with interpretation of small-fires recorded in the main image, simply adding very marginally to the background for the main image. The wedge will be tilted at least a few degrees, with respect to the telescope axis, to avoid generation of significant stray light due to double-reflections with the filters and detector.

### Dichroic option to register two MWIR bands

In the baseline design, the two MWIR bands will be separated along-track by approximately 2.2mm in the primary image plane. This corresponds to a  $0.32^\circ$  along-track angle, equivalent to a 4.6km separation on ground, and a temporal misregistration of 0.7s. This is not necessarily a significant concern since use of multiple detector rows with asynchronous detector read-out, as outlined above, will allow any fire to be imaged close to the center of an identifiable detector element in each of the two MWIR bands, allowing effective spatial registration between the bands in theory to <10% of the pixel dimensions. Temporal registration is a concern mainly for registration with a visible channel for identification of sun-glint from flat surfaces, but registration with a visible channel is essential only for one of the two MWIR bands (at the longer wavelengths). However, there will be an option if required to use a fairly simple dichroic design to superimpose two MWIR bands. The arrangement, located immediately outside each of the 8 telescopes, is sketched in Figure 10. The dichroic transmits the 4653nm band and reflects the 3150nm band. The dichroic plate is plane-parallel, introducing no angular deflection or aberration. The mirror is angled approximately  $0.16^\circ$  along-track with respect to the dichroic, to correct the  $0.32^\circ$  along-track misregistration of the two MWIR bands. Typically, the dichroic can be designed to allow very low transmission of the 3150nm band, so that only the 4653nm band is on the transmitted path. The dichroic may reflect a small percentage of the 4653nm band; this can be reduced by making the mirror coating a dielectric stack with low reflection in the 4563nm band.

### 3.3 Visible channel definition

A visible channel will be included, as outlined in 2.4, to allow identification of false fire detections due to sun glint. A visible channel will also provide context for detected fires and may also be useful in detection of cloud cover. For sun glint detection, the visible channel must be spatially registered with at least one of the IR channels, since sun glint can be transient: the likely preference is registration with the longer MWIR band (at 4653nm). The along-track field imaged by one MWIR channel, in the current design, is approximately  $0.25^\circ$ . Conveniently this is about half of the sun subtense, so that a sun glint detected by a registered visible channel will be imaged close to the center of an MWIR pixel at near-maximum signal level. Initial thresholding, to detect fires while excluding sun glints, can apply:

- a) a maximum for the visible signal, corresponding to a diffuse-equivalent reflectance of 120%,
- b) a minimum signal in the longer MWIR band (BT with respect to average background).

There are advantages in providing spatial sampling for the visible band that is substantially finer than that of the MWIR bands. Resampling of over-sampled data in the visible channel can be used to provide good registration with MWIR data and fine spatial sampling in the visible band can provide improved performance particularly in discrimination against small sun glint areas.

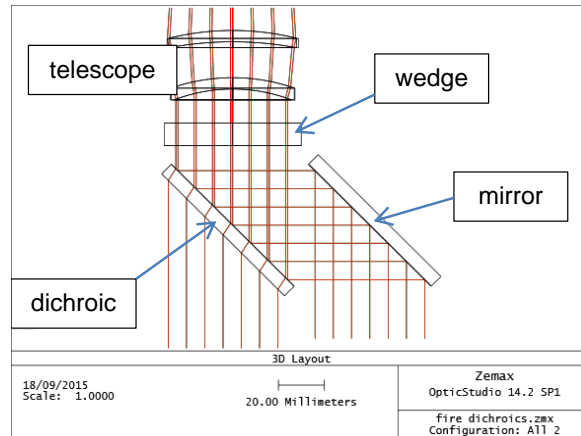


Figure 10: Additions to each telescope showing (a) uncoated zinc sulphide wedge used to add ghost images (b) option on a dichroic and mirror to superimpose ground images in two MWIR bands.

### 3.4 Baseline visible sub-system design

A visible sub-system added to the MWIR system described in 3.2 above will preferably provide a GSD <50m over a 1000km swath width. The likely option is a simple pushbroom imager, using linear CCD arrays. For example two e2v CCD 21-40 arrays with 8µm square elements will provide a total of 24,000 samples across the swath. Provisionally, two arrays will be used with separate lenses. A preliminary design is shown in Figure 11. The focal length of each lens is 167mm, giving a nominal 39m GSD at nadir with 8µm detector elements. The entrance aperture diameters are set at 20mm. Resolution of the optics is diffraction limited over a spectral band from 500nm to 600nm.

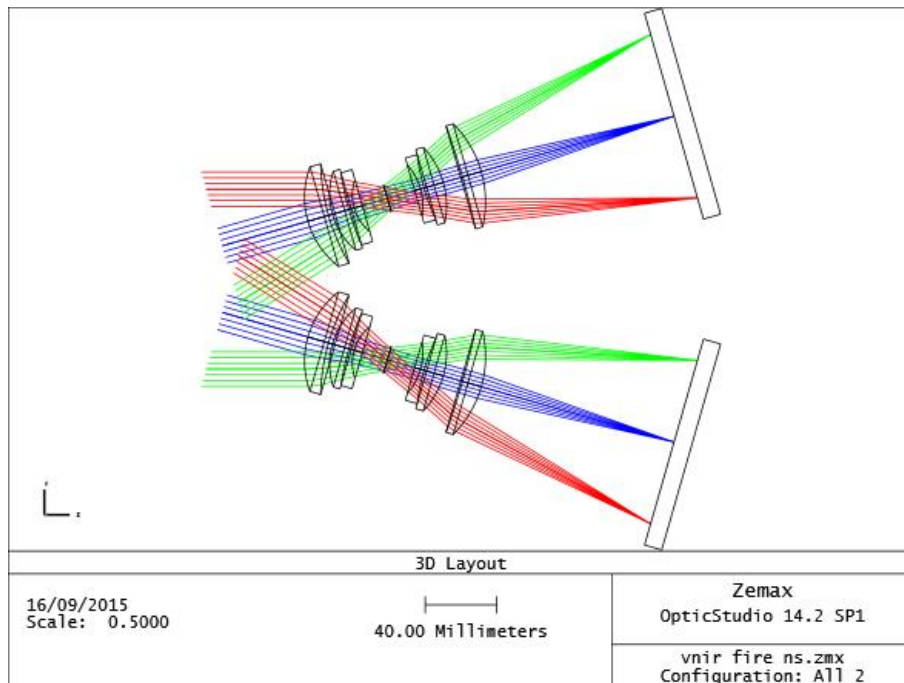


Figure 11: visible channel optics

### 3.5 Thermal control for MWIR optics and detection system

#### Detector cooling

In principle, a SuperHawk detector could be operated at a temperature of at least 175K: at this level, dark signal would reach only 3% of saturation, and the noise on dark signal would be similar to the estimated read noise (nominally 400 rms electrons). Passive cooling can be considered. However, there is provisional preference for use of an active cooler (typically supplied as part of a unit including the detector), which will allow greater flexibility in operation and can easily cool to lower temperatures. Provisionally, the operating temperature is set at 150K.

#### Optics cooling and background thermal signal

Background thermal radiation from instrument structures, reaching the detector, will introduce offset signals. It will be desirable to reduce the thermal background signal to levels comparable with (or below) useful signals from the scene, so that the offsets do not significantly degrade dynamic range or signal to noise ratios. Different temperature control requirements relate to three cavities within the optics system:

- **The dewar** subtends a large solid angle at the detector (nominally 2.7 steradians with obliquity weighting), and will radiate onto the detector over all wavelengths up to the detector cut-off (nominally 5 $\mu$ m), since no filters are placed close to the detector. However, the dewar will be cooled as part of the detector assembly (at 150K), so that its background contribution will be negligible.
- **The relay enclosure** between the filters and the dewar subtends a smaller solid angle at the detector (0.43 steradians) but will also radiate onto the detector at all wavelengths up to the detector cut-off. The relay lens itself will have low emissivity, so that bulk emission is a minor factor. Stray reflection from the filters will be strong and broadband, presenting a major potential problem. The solution is to arrange that the system is telecentric at the filters, and the filters are orthogonal to the transmitted (and reflected) beams. The thermal radiation reflected to the detector from the filter aperture derives from the dewar face and the detector itself, so that the direct filter reflection is therefore not significant. The main residual thermal background is due to stray reflections from the lens surfaces, including double reflections with the filters deriving from relay and cavity structure treated as a black body. The total effective transmission for these contributions is determined by the number of stray-reflecting lens surfaces and their reflection factors (typically reduced to <0.5% per surface by anti-reflection coatings). An effective transmission factor from relay and cavity structure is estimated at 10%. Given this estimate, the background signal from the cavity can be calculated as a function of cavity temperature. A desirable temperature for the relay cavity is provisionally set at 250K, which would reduce the background signal to around the scene signals from a scene at 300K. Options for cooling the relay cavity include (a) conductive cooling via the detector assembly and (b) addition of a small passive radiator (typically 0.01m<sup>2</sup>).
- **The optics and structures outside the filters** also subtend 0.43 steradians at the detector, but can radiate significantly onto the detector only in the filter pass bands. The beam received from outside the filters has a direct path through transmitting prisms and mirrors, which will have low emissivity. No structures are within a direct view of the detector via the relay optics. However, there will be a component of background radiation due to stray reflections from refracting surfaces. Generally, refracting surfaces will be anti-reflection coated, but there will be a significant contribution due to stray reflection from the tilted-wedge ghost-image generator described above, which may reflect up to about 30% of the thermal emittance of the telescope barrels. With this contribution, thermal background signal levels from optics/structure outside the filters will be in the region of 50% of the signal from the scene, if the telescope temperature is similar to the scene temperature. In principle, some cooling of optics outside the filters will be desirable, but a temperature up to 300K is likely to be tolerable. In practice the outer optics will probably run relatively cold, due to radiant heat loss to cold Earth. At present, temperature control for the outer optics and structure is not considered likely to present significant difficulties.

### 3.6 Payload electronics

Payload electronics have not been detailed. Functions of front-end electronics (FEE) will include at least: detector control and drive, and detector signal conditioning and digitisation. An instrument control unit (ICU) will probably be responsible for command, controls, transmission of data to storage, power conditioning and instrument thermal control (monitoring of thermistors and heater control if necessary). Digital data processing will be required to reduce raw sensor data for storage and transmission. The processing may be formally a function of the ICU, but some processing can also be provided within the FEE. As a baseline, the on-board processing will comprise:

- Thresholding (by algorithms to be developed in detail) to identify fires,

- Dumping of data outside areas typically >2km from identified fire pixels.

Data processing could in principle include identification of cloud pixels and generation of cloud outline maps, using visible and MWIR data to identify extended bright and/or cold areas.

### 3.7 Radiometric and geometric calibration

Radiometric calibration of the sensor has not been considered in detail. Fire identification and power measurement depend on detection of brightness temperature differences between MWIR bands typically of >10K and brightness temperatures differences with respect to local background. It is unlikely to be useful to measure absolute brightness temperatures to better than a few K. Inter-band relative accuracy to order of 1K is probably desirable. Absolute and relative calibration to these levels will almost certainly be achieved using vicarious calibration in flight, for example over a selected ocean area for a cold level and desert for a warm level. The visible sub-system is required critically to detect sun-glint at levels substantially above a high albedo threshold. Accuracy for albedo measurements better than 10% will probably be adequate. Vicarious calibration will again be expected to suffice, probably using an eclipse image as a dark level and desert as a bright level. Results from vicarious calibration will update calibration data files generated pre-flight. Pre-flight radiometric calibration will be performed at pixel level, using black body sources for MWIR bands and a calibrated integrating sphere for the visible band. It will cover operation for a range of optics and detector temperatures, and will include characterization the ghost images used to extend the dynamic range in MWIR bands.

Relative spatial radiometric response and dark-level non-uniformity will be measured conventionally in flight, for both MWIR and visible bands, by detection of banding in extended images. Further development is unlikely to include on-board sources outside telescope apertures, but further study may indicate a use for internal “stim lamp” sources to measure response drifts over periods between vicarious calibrations. Conventional methods for measurement of dark level drift over sub-orbital periods will include measurement of signals from masked pixel and possibly from over-scan (dummy-read) pixels.

Pre-flight geometric calibration will include at least:

- measurements on enclosed energies for all bands, at representative points in the field,
- detailed mapping of pixel numbers in all bands against along-track and across-track field angles, with respect to sensor reference features,
- spatial registration between fields and bands.

Correlation of image data between sub-fields and bands will be used to update pre-flight registration data.

## 4. SYSTEM DESIGN SUMMARY AND PERFORMANCE

### 4.1 MWIR system summary

Design parameters of the baseline MWIR system, and assumption for radiometric analysis, are summarized in Table 1, with the principle results of radiometric performance analysis. The most powerful fires are expected to saturate the detector, as discussed in 3.2, which leads to inclusion of a ghost-image generator allowing high intensities to be measured.

#### Radiometric resolution

Radiometric resolution of the system is calculated for Table 1 in terms of noise-equivalent temperature differences (NEdT<sub>s</sub>). The values relate to single spatial/spectral samples – NEdT<sub>s</sub> will eventually be improved by processing data from around 40 samples for each ground point and band. Radiometric resolution is not expected to limit system performance in identification of fires or measurement of fire radiative powers and temperatures, since achievable NEdT<sub>s</sub> will generally be below the levels of background temperature non-uniformity, and the accuracies required in brightness temperatures and brightness temperature differences. In principle, a system with smaller aperture could be used for radiometric resolution; however, the current design aperture is required for spatial resolution close to the diffraction limit.

**Table 1 MWIR system summary and radiometric resolution**

Parameter	Value
GSD at altitude 814km	100 m
Dwell period (adjusted to de-synchronise)	13 ms
Aperture diameter	48 mm
Focal length (telescope + relay)	65 mm
Detector element size	8 $\mu\text{m}$
Spectral band 1	3510 nm $\pm$ 20 nm
Spectral band 2	4653 nm $\pm$ 20 nm
Reference scene temperature	300 K
Reference fire fractional area	0.001
Maximum fire temperature	1350 K
Minimum fire temperature	650 K
Optics transmission from scene	50%
Quantum efficiency	80%
Read noise	400 e- rms
Detector temperature	150K
Detector saturation	5 Me-
Background thermal radiation parameters	
Optics transmission from cool structures	5%
Cool structure (after filters) emissivity	1
Cool structure (after filters) temperature	250K
Dewar aperture	f/1.36
Dewar temperature	150 K
Detector cut-off wavelength	5000 nm
<b>Radiometric resolution</b>	
NEdT for scene at 300K, single pixel – band 1	480 mK
NEdT for scene at 300K, single pixel – band 2	90 mK

#### MWIR spatial resolution

Enclosed energy for a sub-pixel fire will be limited by diffraction. The theoretical enclosed energy in the 8 $\mu\text{m}$  square detector element, for a centered fire is 67% for the 4651nm band and 82% for the 3150nm band. Enclosed energy will be reduced by along-track motion during the integration period. Calculated enclosed energy with the baseline integration period (equivalent to 7 microns in the image plane) is 58% in the 4651nm band. Spatial oversampling of data will be expected to ensure that there will be at least one sample with an effectively-centered potential-fire (or potential solar reflection) that can be used in preliminary thresholding. Following preliminary identification of a fire, it is likely that processing of around 40 samples for each band and field point will be used, in more precise secondary thresholding and in eventual estimation of FRPs and temperatures.

#### 4.2 Visible sub-system summary

Design parameters of the baseline visible sub-system, are summarized in Table 2, with the principle results of radiometric performance analysis. The detector will not saturate at diffuser-equivalent albedo values up to approximately 500%, and signal to noise ratios will be more than adequate for the glint-detection purpose. As for the MWIR system, a smaller aperture could be justified considering the radiometric requirements; however, diffraction at a much smaller aperture would begin to reduce effective resolution.

Table 2: Design summary and radiometric analysis results for the visible sub-system

Parameter	Value
GSD at altitude 814km	39 m
Dwell period with x2 along-track over-sampling	3.0 ms
Aperture diameter	20 mm
Focal length	167 mm
Spectral band	500nm - 600nm
Solar irradiance in band	1.8 W.m <sup>-2</sup> .nm <sup>-1</sup>
Optics transmission	90%
Quantum efficiency	50%
Read noise	40 e- rms
“Maximum” albedo	120%
“Reference” albedo	20%
Detector saturation level	400,000 e-
<b>Radiometric results</b>	
Signal % of saturation at maximum albedo	12%
SNR at reference albedo (single sample)	75

### 4.3 System performance in fire detection and analysis

#### Minimum detectable fire power

System performance in detection and analysis of fires, using two MWIR bands with a visible channel, will preferably be subject to a more extensive theoretical study, which may require some support from experiments. The uncertainties to be investigated include effects of:

- spectral variations in sun glint reflectances
- spectral variations in MWIR emissivities
- non-uniformities in ground temperature
- spectral variations in atmosphere transmission

Based on the simple analysis above, a system with 100m GSD in MWIR bands (and 40m GSD in a visible band) is likely to provide positive identification of fires with FRPs above 0.5MW to 1MW. This estimate applies to fires seen in daylight; thresholds are strongly affected by the need to exclude sun glints, so that smaller fires will be identified at night.

### 4.4 Payload budgets

No structure design or electronics design has been generated so far. Estimated payload budgets are listed in Table 3. The estimates for recorded data are based on the assumption that all data within 2km along- and across-track of a fire pixel are retained. For the MWIR bands, this also includes multiple samples (frames) for each point in the area. For total data recorded per orbit, data in this 4km square area will of course be multiplied by an estimate of the total number of fires seen in an orbit, taking account of clumping of fires or extended fires.

Table 3: Payload budget estimates

	MWIR sub-system	Visible sub-system
<b>Optics dimensions without structure</b>		
Along-track	500mm	60mm
Across-track	500mm	300mm
Nadir	250mm	250mm
<b>Power</b>		
Detector + FEE	10W	10W
Cooler	10W	
Temperature control	2.5W	2.5W
Total power	22.5W	12.5W
<b>Data</b>		
Digitization	14 bits	14 bits
Raw data rate	63 Mpixels/s	3.8 Mpixels/s
Rows recorded per fire	40	1
Columns recorded per fire	40	100
Frames recorded per fire	50	100
Data recorded per fire	1120 Kbits	140 Kbits

## 5. CONCLUSIONS

The paper investigates selection of spectral bands for a sensor detecting fires from a satellite in low-Earth Orbit, concluding that a system using two Mid-Wave Infrared bands, with a visible channel, will have significant advantages with respect to the more common use of a Long-Wave band with a Mid-Wave band. A detailed optical design is described that allows a single Mid-Wave area-array detector to cover a 1000km swath at 100m ground sample distance. This will allow detection and measurement of fires having minimum radiant powers of 0.5MW to 1MW.

## ACKNOWLEDGEMENTS

The paper describes work performed by Surrey Satellite Technology Ltd on an electro-optical sensor design for fire measurement from space, with support on fire science from Martin Wooster of University College London. The work was funded by the European Space Agency, as one of a set of studies on potential missions operating in convoy with the ESA Sentinel platforms.

## REFERENCES

- [1] Sentinel Convoy for Land Processes Task 1: Critical Review and Gap Analysis. SCL-ULE-TN-02\_V4.0. Rev 1. (23/01/2012).
- [2] M. J. Wooster, Xu, and Nightingale (2012). Sentinel-3 SLSTR active fire detection and FRP product: Pre-launch algorithm development and performance evaluation using MODIS and ASTER datasets; Remote sensing of environment 120 236-254.
- [3] Dennison, P. E., Charoensiri, K., Roberts, D. A., Peterson, S. H., & Green, R. O. (2006). Wildfire temperature and land cover modeling using hyperspectral data. Remote Sensing of Environment, 100(2), 212-222

- [4] Wooster, M. J., Roberts, G., Perry, G. L. W., & Kaufman, Y. J. (2005). Retrieval of biomass combustion rates and totals from fire radiative power observations: FRP derivation and calibration relationships between biomass consumption and fire radiative energy release. *Journal of Geophysical Research: Atmospheres* (1984-2012), 110(D24).
- [5] Sobrino, J. A., Mattar, C., Pardo, P., Jimenez-Munoz, J. C., Hook, S. J., Baldrige, A., & Ibanez, R. (2009). Soil emissivity and reflectance spectra measurements. *Applied optics*, 48(19), 3664-3670.
- [6] Johnston, J. M., Wooster, M. J., & Lynham, T. J. (2014). Experimental confirmation of the MWIR and LWIR grey body assumption for vegetation fire flame emissivity. *International journal of wildland fire*, 23(4), 463-479.
- [7] Realmuto, V. J., Dennison, P. E., Foote, M., Ramsey, M. S., Wooster, M. J., & Wright, R. (2015). Specifying the saturation temperature for the HypsIRI 4- $\mu$ m channel. *Remote Sensing of Environment*, in press.